6 Lattice Design

6.1 Rev. 1-Lattice with Resistive Combined Function Magnets Inside the Detectors

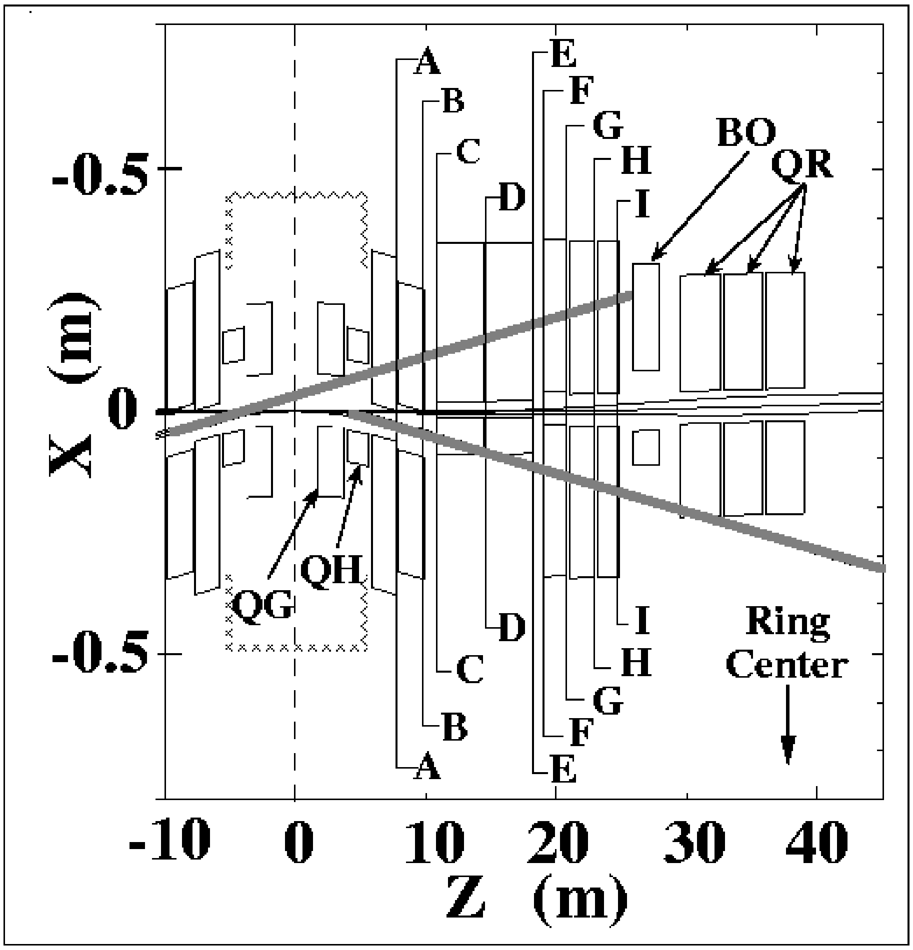

Figure 5: Expanded view of Rev. 1 layout with cross section cuts, **AA** through **II**, indicated for use in aperture plots in Figures 8–17 and Tables 2–4. The sections, ordered with respect to the electron direction, are: **AA** = downstream QI, **BB** = downstream QJ, **CC** = upstream QM1, **DD** = downstream QM1 and upstream QM2, **EE** = downstream QM2,**FF** = upstream QN1, **GG** = downstream QN1,**HH** = downstream QN2 and **II** = downstream QN3.

6.1.1 Rev. 1 Interaction Region Geometry

The Rev. 1 layout for the central ±40 mm on either side of the IP is shown in Fig. 4. The magnet positions and lattice optics are symmetric about the IP. Separation of the electron and proton beam is accomplished via two pairs of combined function magnets, QG and QH, which are located inside of the ZEUS and H1 experimental detectors.

The QG magnet deflects the electron beam by 3.66 mrad, while QH gives an additional 4.24 mrad for a total separation angle of 8 mrad. The total deflection is apportioned between

QG and QH such that QG is "softer" with an average field at the electron closed orbit of 0.185 T as compared to the QH average of 0.261 T. The QG and QH magnets deflect the proton beam by ≈0.30 mrad according to the proton to electron magnetic rigidity ratio of ≈27 to 1.

The critical energy for synchrotron radiation coming from QG is intentionally lower than that for QH as this lowers the synchrotron radiation photon critical energy thus helps to reduce backscattering from the closest synchrotron radiation absorber at 11m. As addressed in the next subsection, the QG and QH magnets also provide additional focusing in order to reduce the vertical chromaticity in the e–ring.

The next quadrupoles, QI and QJ, are centered on the electron beam in order to minimize their contribution to the synchrotron radiation fan passing through the detector and the downstream magnets out to the last QN quadrupole. Because there is a significant e–p beam separation already in QI and QJ, these magnets also deflect the the proton beam. The change in this proton deflection during electron ramping as well as that due to the QG and QH magnets must be compensated by a proton closed orbit bump,

At $z = 11$ m the e–p beam separation is sufficient to start strongly focusing the proton beam in the first QM half–quadrupole while letting the electron beam pass virtually unaffected as it passes through a deep notch cut–out in the QM mirror plate. After exiting a second QM magnetic septum quadrupole the e–p separation is sufficient to use a new current septum quadrupole, type QN. In the QN current septum quadrupoles there is a high–current density septum coil between the e and p beams.

Note that because the proton beam must by definition transit the QM quadrupole away from the magnetic symmetry point, the QM magnets also act as combined function magnets in deflecting the proton beam. The QN quadrupoles, unlike the QM half–quadrupoles discussed above, provide a full aperture for the proton beam and could in principle be centered on the proton closed orbit in order not to give any additional deflection to the protons. In practice the magnetic axis at the nearest end of the first of three QN quadrupoles is shifted horizontally outward in order to provide more clearance between the e–beam and the current septum as will be discussed in the next subsection; however, a side effect of the resulting horizontal offset and rotation of the first QN magnet is that it also deflects the proton beam.

The combination of two QM quadrupoles and three QN quadrupoles provides the necessary interaction region vertical focusing. The necessary horizontal focusing is provided by a series of HERA–standard QR quadrupole magnets. The QR magnets are reused from the existing HERA interaction region configurations.

The one proviso in reusing these QR magnets is that the e–p beam separation is not as large at these magnets as in the present HERA configuration. This has consequences for the innermost QR magnets. The mid-plane clamping structure will have to be ground away on the ring–inside side and replaced with clamping with sufficient clearance to permit installation of the electron beam pipe immediately alongside these magnets.

Between the last QN and the first QR space is allocated in the p–ring for a horizontally bending dipole, BO. BO is needed to help compensate the off–axis steering of the proton beam in the previous QG, QH, QI, QJ, QM and QN quadrupoles. Between BO and the first QR quadrupole at 29 m, there is space for an existing e–ring quadrupole, QK (QK is not shown on Fig. 4).

For future reference the beam and magnet offsets at some critical locations are tabulated in Table 2 according at the positions indicated in Fig. 5.

Section ID	Description	Distance (m)	Magnet Center (mm)	p–beam Center (mm)	e–beam Center (mm)
—	IP	0.00	—	0.0	0.0
AA	End QI	7.72	-30.3	-1.2	-30.3
BB	End QJ	9.90	-47.7	-1.9	-47.7
CC	Begin QM1	11.00	-13.0†	-1.9	-56.5
DD	End QM1	14.50	-14.0†	-1.5	-84.5
EE	End QM2	18.20	-14.4†	0.4	-114.
FF	Begin QN1	19.00	10.5	1.0	-120.
GG	End QN1	20.80	4.5	2.2	-135.
HH	End QN2	22.80	4.0	2.8	-143.
II	End QN3	24.90	4.0	4.0	-160.

Table 2: Rev. 1 Lattice Offsets with Luminosity Optics. The section IDs are as shown in Fig. 5. † For the magnetic septum half–quadrupoles, QM1 and QM2, magnet center is on the inner surface of the mirror plate.

6.1.2 Rev. 1 Interaction Region Luminosity Optics

The Rev. 1 luminosity optics for electrons is shown in Fig. 6. The electrons are focused in an effective triplet combination with QG and QH providing the initial vertical focusing, QI the horizontal focusing and QJ more vertical focusing. The electron focusing is completed within 10 m from the IP.

The maximum electron horizontal β_x^{max} =127. m occurs near the middle of QI while the maximum electron vertical β_y^{max} =350. m occurs near the end of QJ. There are several proton quadrupoles, types QM and QN, with septa in the 18.2 m gap between QJ and QK; however, because the electrons pass through the "field free" region these magnets have no effect on the electron beam and are not shown. In reality there are transverse fields of $\approx$ few gauss at the electron closed orbit in the septum magnets and therefore they will have a small effect on the electrons. Note that in the 14 m drift from 11 to 25 m the electron horizontal–β is kept almost constant to a value below about 45. m in order to maintain the desired $\pm 20\sigma$ for electrons in spite of the close proximity of the septa in the proton septum quadrupoles.

The luminosity inner aperture requirements for the QG and QH are set by a combination of electron orbit offset, horizontal electron beam size and especially for the electron–downstream QG and QH magnets by the need to pass the synchrotron radiation fan from the upstream QG and QH magnets. The inner aperture requirements for QI and QJ are set by the increasing large e–p horizontal beam separation in these quadrupoles and the vertical aperture requirements for protons. Aperture requirements are addressed in more detail in the next subsection.

The electron horizontal and vertical dispersion and their slopes (not shown on Fig. 6) at the IP are zero. Outside the separator magnets QG and QH the horizontal dispersion slowly changes, associated with the 8 mrad horizontal separation angle, reaching 0.12 m at 25 m from the IP.

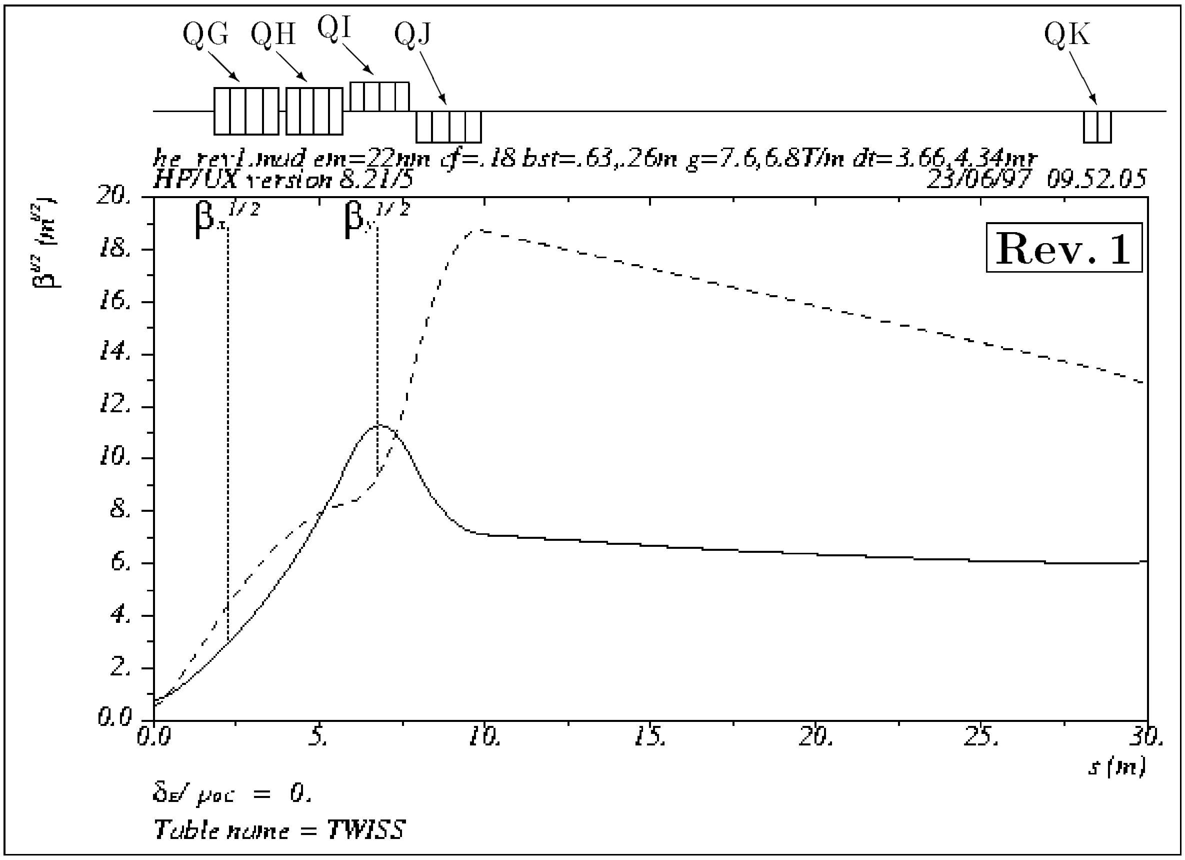

Figure 6: Rev. 1 Electron Lattice Luminosity Optics. Since the Rev. 1 lattice is symmetric with respect to the IP, lattice functions for only the left half are shown. $\sqrt{\beta_x}$ (solid line) and $\sqrt{\beta_y}$ (dashed line) are plotted as a function of distance, S, from the IP. Note that the maximum horizontal β_x^{max} =127. m occurs near the middle of QI while the maximum vertical β_y^{max} =350. m occurs near the end of QJ. There are several proton quadrupoles, types QM and QN, with septa in the 18.2 m gap between QJ and QK; however, because the electrons pass through the "field free" region these magnets have no effect on the electron beam and are not shown. In reality there are transverse fields of ≈ few gauss at the electron closed orbit in the septum magnets and therefore they will have a small effect on the electrons, especially with respect to e–polarization optimization.

The Rev. 1 luminosity optics for protons is shown in Fig. 7. The electron quadrupoles QG, QH, QI and QJ have very little effect on the proton beam. The strong focusing for the protons starts at 11 m from the IP with the start of the first magnetic septum quadrupole, QM. In contrast to the triplet focusing combination for the electrons, the protons are focused in a doublet combination. The inner vertical focusing is provided by the combination of two magnetic septum quadrupoles, QM1-2, and three PEP–II style current septum quadrupoles, QN1-3. The horizontal focusing is done with four HERA QR–type quadrupoles relocated from their original positions in the HERA proton ring.

Note that the maximum horizontal β_x^{max} =1335. m occurs near the middle of the first QN quadrupole while the maximum vertical β_y^{max} =2000. m occurs in the second QR quadrupole.

The interaction region luminosity layout and optics are intended to be the same for ZEUS and H1; however, in detail there are small optical differences which are due to the different detector solenoid parameters in the two experiments. In particular the H1 solenoid is not

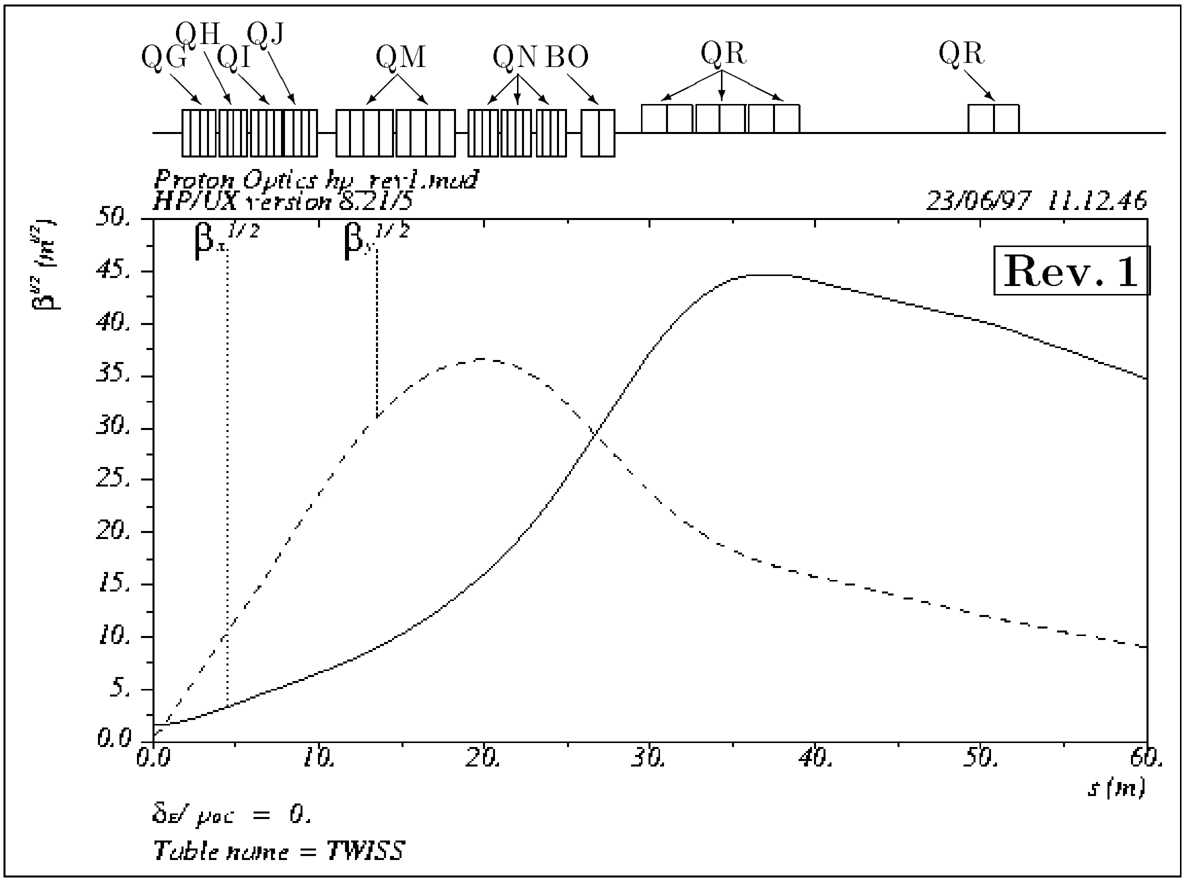

Figure 7: Rev. 1 Proton Lattice Luminosity Optics. Since the Rev. 1 lattice is symmetric with respect to the IP, lattice functions for only the left half are shown. $\sqrt{\beta_x}$ (solid line) and $\sqrt{\beta_y}$ (dashed line) are plotted as a function of distance, S, from the IP. Note that the maximum horizontal β_x^{max} =1335. m occurs near the middle of the first QN quadrupole while the maximum vertical β_y^{max} =2000. m occurs in the second QR quadrupole.

longitudinally symmetric with respect to the IP and this along with its intrinsically different integrated strength means that there are small optic couplings, asymmetries and orbit distortions which are slightly different between the two experiments. These issues are dealt with in more detail in later sections.

Horizontal and vertical β–functions for the Rev. 1 electron and proton luminosity optics lattices are given in Table 3 for the locations indicated on Fig. 5.

6.1.3 Rev. 1 Interaction Region Required Apertures for Luminosity Optics

Here we present aperture requirements for the new electron and proton quadrupoles QI, QJ, QM and QN for the Rev. 1 luminosity optics. Aperture requirements for the magnets inside the experimental detectors are discussed separately for ZEUS and H1 in the respective experimental impact subsections and for the new Rev. 2 superconducting magnets QG, QH and QO in their own Rev. 2 subsection. Optics and the associated required apertures for electron and proton beam injection and ramping are also treated in later subsections. Also since the most stringent design requirements for the QI, QJ, QM and QN magnets stem from the need to accommodate

Section ID	Description	Distance (m)	Proton β_x (m)	Proton β_y (m)	Electron β_x (m)	Electron β_y (m)
—	IP	0.00	2.45	0.18	0.63	0.26
AA	End QI	7.72	27.0	348.	102.	163.
BB	End QJ	9.90	42.0	551.	50.5	350.
CC	Begin QM1	11.00	51.5	677.	49.0	338.
DD	End QM1	14.50	96.6	1064.	45.1	303.
EE	End QM2	18.20	189.	1300.	41.7	267.
FF	Begin QN1	19.00	217.	1321.	41.0	260.
GG	End QN1	20.80	298.	1321.	39.7	244.
HH	End QN2	22.80	363.	1286.	39.0	234.
II	End QN3	24.90	534.	1137.	38.0	216.

Table 3: Rev. 1 Lattice Luminosity Optics The section IDs are as shown in Fig. 5.

the downstream synchrotron radiation fans from the upstream separator magnets, we focus on the critical electron–downstream positions AA through II indicated on Fig. 5.

Some assumptions and boundary conditions for the Rev. 1 aperture calculations are as follows:

- In order to achieve reasonable experimental background levels $\pm 20\sigma$ should be available for electrons and $\pm 12.5\sigma$ for protons.
- The proton normalized emittance of 5πmm·mrad is used for both the horizontal and vertical planes.
- By increasing the horizontal focusing in the arc cells of the e–ring the electron horizontal emittance is brought to 22πnm·rad.
- An 18% vertical to horizontal emittance ratio is used in establishing matched electron and proton spot sizes at the IP.
- Except as noted for the QM and QN septum synchrotron radiation absorber masks, the synchrotron radiation fan coming from the separator dipoles is able to pass unhindered up to 25 m from the IP.

Numerical values for the 6σ horizontal and vertical proton and electron beam sizes for the above beam emittances and the optical functions from Table 3 are tabulated for reference in Table 4. With respect to a coordinate system aligned along the extension of the e–p collision axis, the horizontal offsets for the magnets, proton and electron beam are given for the Rev. 1 geometry described earlier in Table 2 for each of the longitudinal sections defined on Fig. 5.

In the following Figures 8–17 magnet pole and coil profiles are taken to be consistent with the existing 2–dimensional magnet profiles used for the field calculations done for the later magnet definition subsection; however, the indicated vacuum chamber profiles are drawn in freehand as a guide to one's eye and should not be taken to indicate a specific mechanical design choice or stress estimation. In all of these Rev. 1 aperture plots there is at least 2 mm space available for the vacuum chamber while maintaining the indicated $\pm 20\sigma$ electron and $\pm 12.5\sigma$ proton beam profiles.

For the Rev. 1 luminosity optics the tightest aperture for protons occurs with section **EE**, the downstream end of the second QM quadrupole. At this point there is almost exactly 2 mm transverse space between the $\pm 12.5\sigma$ proton beam ellipse and the QM pole and mirror plate. The tightest electron aperture occurs at the next section cut **FF**, the upstream end of the first QN At this point there is almost exactly 2 mm between the 20σ electron beam ellipse and the septum coil.

As an indication as to how the synchrotron radiation fan from the separator magnets spreads out in the horizontal and vertical planes the $3\,\sigma$ synchrotron radiation beam from both the upstream and downstream separator magnets is shown (but not labeled) spreading across the mid plane of these plots. 3σ is used here to indicate the area containing most of the $\approx$25 kW of synchrotron radiation generated in the separator magnets at 30 GeV electron energy; however, the shadowing of downstream elements by the QM and QN absorber masks is neglected (only affects ring inside fan, negative x). Since the electron beam is centered in the QI and QJ quadrupoles, they are not themselves strong sources of synchrotron radiation. This relatively weak contribution, resulting in a diffuse synchrotron radiation background around the inner and outer synchrotron radiation fan endpoints, is also not shown.

In order to maximize the available aperture in the Rev. 1 luminosity optics, the QM and QN septum magnets are horizontally offset and horizontally rotated as needed. In some cases, which will be noted, this requires that the magnets not be aligned along the nominal electron or proton closed orbits. The extent of these magnet rotations can be inferred from the magnet center positions listed in Table 2 by the fact that some magnets, notably the first QM and QN quadrupoles, have different beginning and ending offsets with respect to the proton beam.

Fig. 8 shows the location of the tightest aperture found in the downstream QI quadrupole, section **AA**. Section **AA** occurs at the downstream end of QI where the electron and proton beam separation is the greatest. The inscribed pole radius for the QI quadrupole is 35 mm and this magnet is centered on the electron closed orbit.

It is clear from Fig. 8 that even though this magnet's primary function is to focus the electron beam, its pole radius is set by proton vertical beam size and the fact that the protons are significantly off axis. Note that even at this first section it is already necessary to split the coil on the ring outside to pass the synchrotron radiation fan.

Here the coil is also shown to be split apart top and bottom as well as on the ring inside in order to maintain some magnetic symmetry for this magnet. Symmetry is desirable only to the extent that the iron in this magnet is very highly saturated and such symmetry is not a firm requirement as long as good field quality is assured in the magnetic design. A minimal non–symmetric vacuum chamber is shown.

Section **BB** in Fig 9 shows an equivalent point at the end of the next electron quadrupole, QJ. QJ is also kept centered on the electron beam so as to generate only minimal additional synchrotron radiation. At section **BB** the proton beam size and e–p beam separation has increased to the point that the assumed 50 mm pole radius is barely sufficient. Again, as with QI, the magnet has to have a split coil on the ring outside in order to pass synchrotron radiation. The magnet is shown in Fig 9 with a symmetric coil configuration and a minimal non-symmetric vacuum beam pipe.

At the next section **CC** in Fig. 10, the beginning of the first QM magnet, the beams are fully separated by a magnetic septum and are in different, though not obviously independent, beam pipes. The beam pipes are joined upstream of this first QM and this joint has to be protected from intense heating by an absorber mask. Since the dominant source of synchrotron radiation backscatter background to the experiment is this absorber at $\approx$11 m, the magnetic septum and associated vacuum beam pipe joint must be kept as horizontally narrow as possible.

Present QM design calculations point to a minimum septum width of about 8–10 mm, driven by the need for a small cross section and low current magnetic field trim coil, and this is not much transverse space for separate electron and proton vacuum flanges.

With sections **CC** through **EE** in Figures 10–13 we see that the horizontal spread of the synchrotron radiation fan continues to grow along with the horizontal proton beam size. In the last section **EE** at the end of the second QM the proton beam ellipse fills all of the available 37 mm half–aperture of the quadrupole, after subtracting 2 mm for vacuum beam pipe. This location that sets 37 mm as the minimum inscribed pole radius for the QM magnets. The proton vacuum beam pipe has an increasingly unfavorable horizontal aspect ratio due to the need to pass the synchrotron radiation; however, on the ring inside the $\pm 20\sigma$ electron beam ellipse has pulled well away from the septum plate and is unrestricted until reaching the next quadrupole, the first QN current septum quadrupole.

Profiles at the beginning of the first QN, section **FF** are shown in Fig. 14. Here the $\pm 20\sigma$ electron ellipse plus 2 mm vacuum beam pipe are right up against the ring inside edge of the QN septum coil. Even this would not be possible if this end of the magnet were not pushed 9.5 mm to the ring outside (i.e. toward the proton beam). Note that in the immediate vicinity of the septum coil, that is, the outer edge of the $\pm 20\sigma$ electron ellipse, the vertical field is expected to be in the range 10–20 gauss but the field drops to only a few gauss close to the electron closed orbit.

The downstream end of this first QN, section GG shown in Fig. 15, is almost centered with respect to the proton beam center as the e–p beam separation is now sufficient to provide the needed space for the electrons.

Although not indicated in Fig 14, the shadow of the synchrotron radiation absorber mask in front of the QM magnet at 11 m cannot fully cover the QN current septum so a second ring inside synchrotron radiation absorber mask is required just upstream of this first QN magnet. This second absorber is thus $\approx$19 m from the IP.

Note that the ring outside coil is also split to pass synchrotron radiation further downstream. This splitting has the unfortunate consequence of spoiling the quadrupole symmetry and thereby leading to a more challenging magnetic design optimization to assure good field quality in this highly saturated magnet.

It might be possible to restore approximate coil symmetry for QN by filling in the ring outside coil mid plane. Of course this coil would then have to be protected by its own absorber mask, similar to that for the coil close to the electrons; however, this would yield some additional experimental backscatter background. Should the ZEUS and H1 synchrotron radiation Monte Carlo calculations show this additional background to be tolerable this option could be implemented. For the Rev. 1 lattice we assume the more "conservative" (from the background viewpoint) QN design option with the out-bound split coil.

Finally in Figures 16 and 17 we see the full extent of the synchrotron radiation fan with sections **GG** through **II** in the second and third QN quadrupoles. With both the second and

Section ID	Description	Distance	Proton		Electron	
			$6\sigma_x$	$6\sigma_y$	$6\sigma_x$	$6\sigma_y$
		(m)	(mm)	(mm)	(mm)	(mm)
—	IP	0.00	1.18	0.32	1.18	0.32
AA	End QI	7.72	2.4	8.5	9.0	4.8
BB	End QJ	9.90	2.9	10.6	6.3	7.1
CC	Begin QM1	11.00	3.2	11.8	6.2	6.9
DD	End QM1	14.50	4.5	14.8	6.0	6.6
EE	End QM2	18.20	6.2	16.4	5.7	6.2
FF	Begin QN1	19.00	6.7	16.5	5.7	6.1
GG	End QN1	20.80	7.8	16.5	5.6	5.9
HH	End QN2	22.80	7.8	16.5	5.6	5.8
II	End QN3	24.90	10.5	15.3	5.5	5.5

Table 4: Rev. 1 Lattice Beam Envelopes with Luminosity Optics. The section IDs are as shown in Fig. 5.

third QN quadrupoles aligned parallel to the e–p collision axis, it is possible to show both the beginning and end electron and proton profiles on the same figures. The synchrotron radiation fan is passed beyond the third QN to the primary synchrotron radiation absorber located at ≈25 m.

With this third QN the proton vertical focusing is completed and we see that the $\pm 12.5\sigma$ proton beam ellipse is finally starting to grow smaller vertically. After this QN the proton beam is focused horizontally in a set of HERA QR–type quadrupoles.

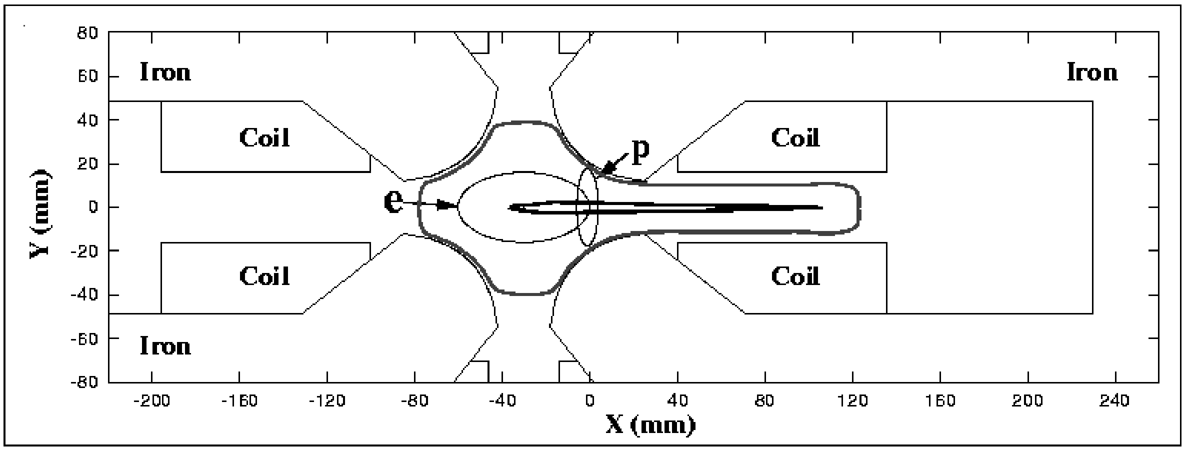

Figure 8: Aperture required at downstream end of QI, Fig. 5 section **AA**.

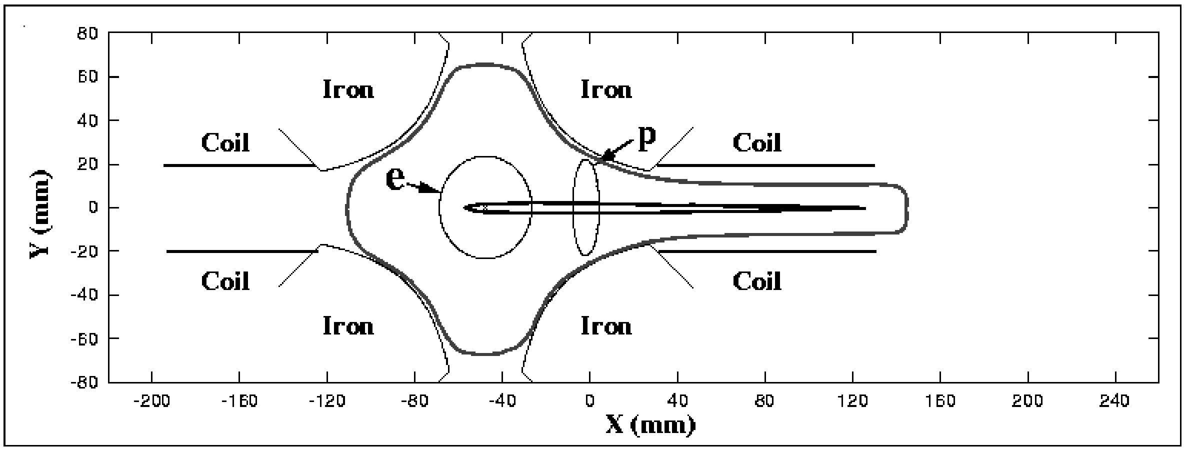

Figure 9: Aperture required at downstream end of QJ, Fig. 5 section **BB**.

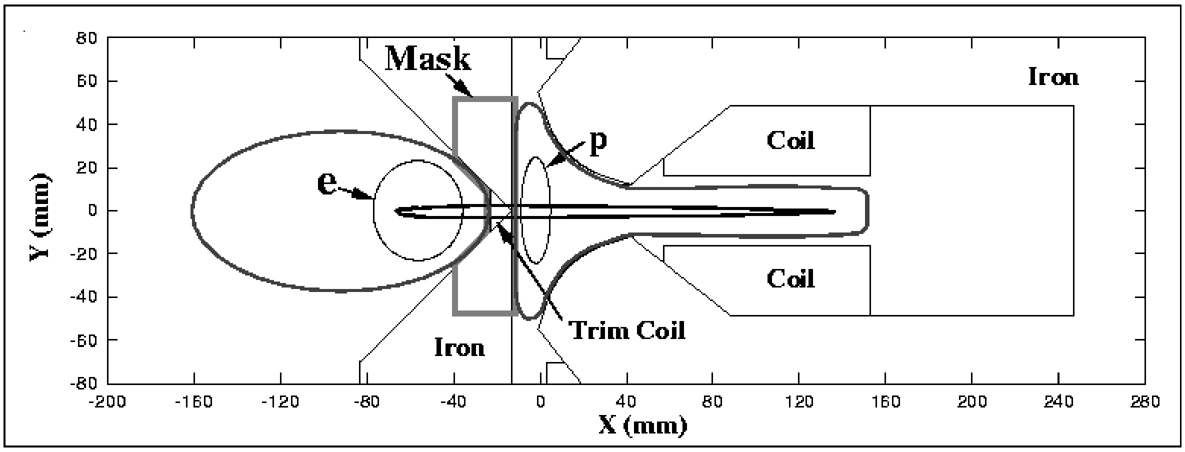

Figure 10: Aperture required at upstream end of first QM, Fig. 5 section **CC**.

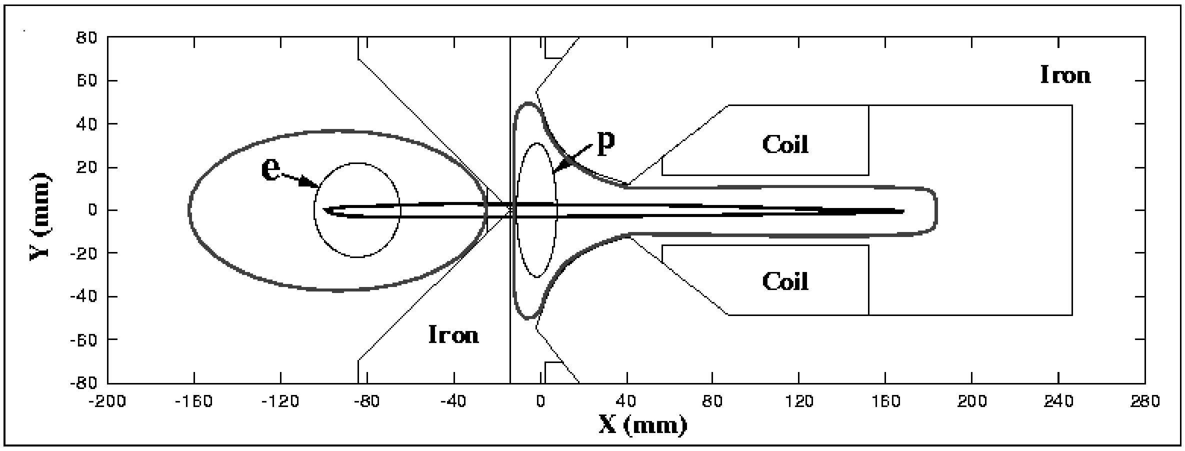

Figure 11: Aperture required at downstream end of first QM, Fig. 5 section **DD**.

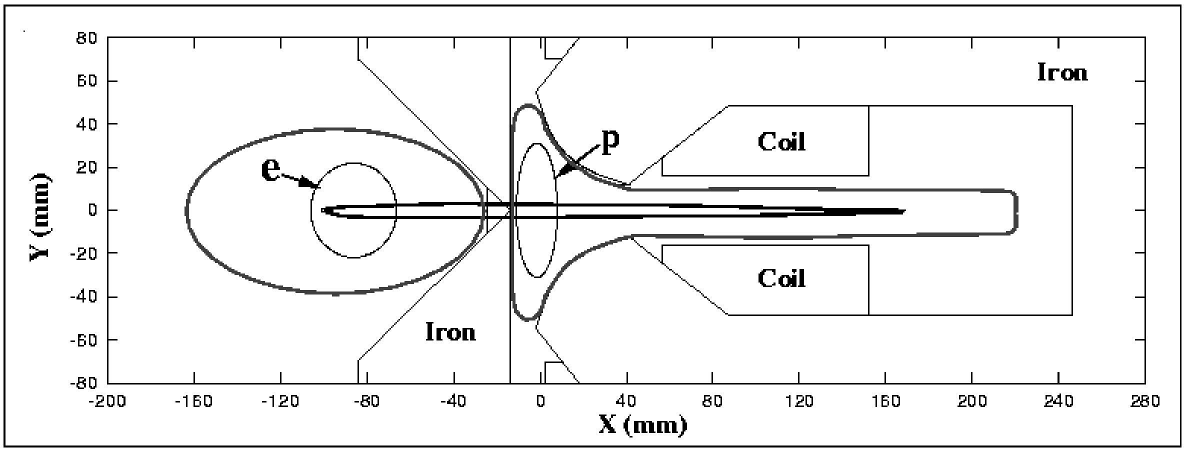

Figure 12: Aperture required at upstream end of second QM, Fig. 5 section **DD**.

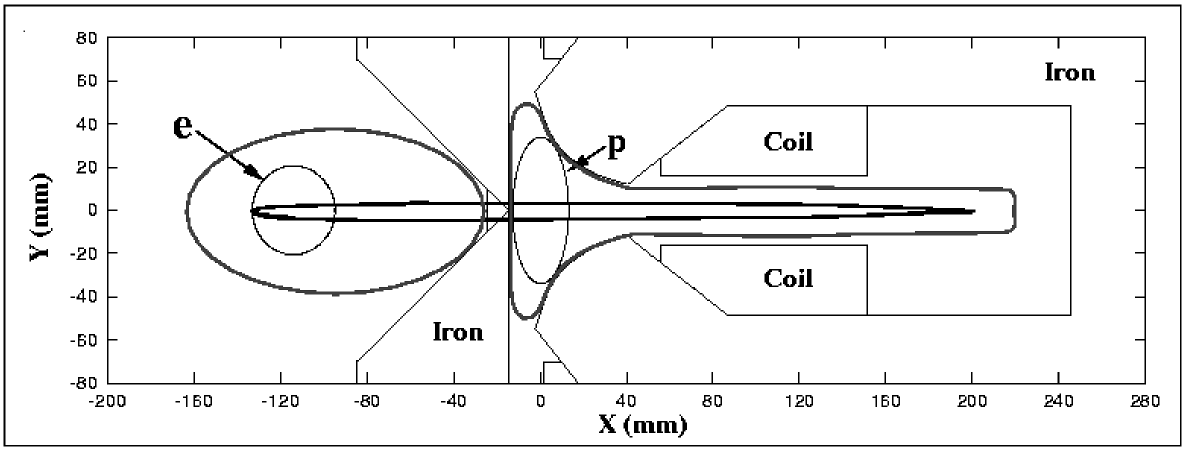

Figure 13: Aperture required at downstream end of second QM, Fig. 5 section **EE**.

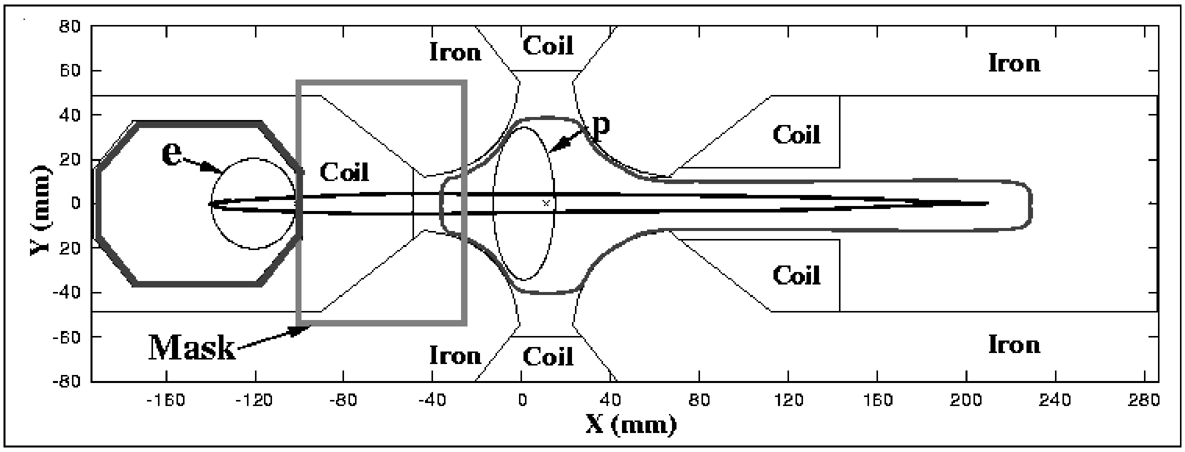

Figure 14: Aperture required at upstream end of first QN, Fig. 5 section **FF**.

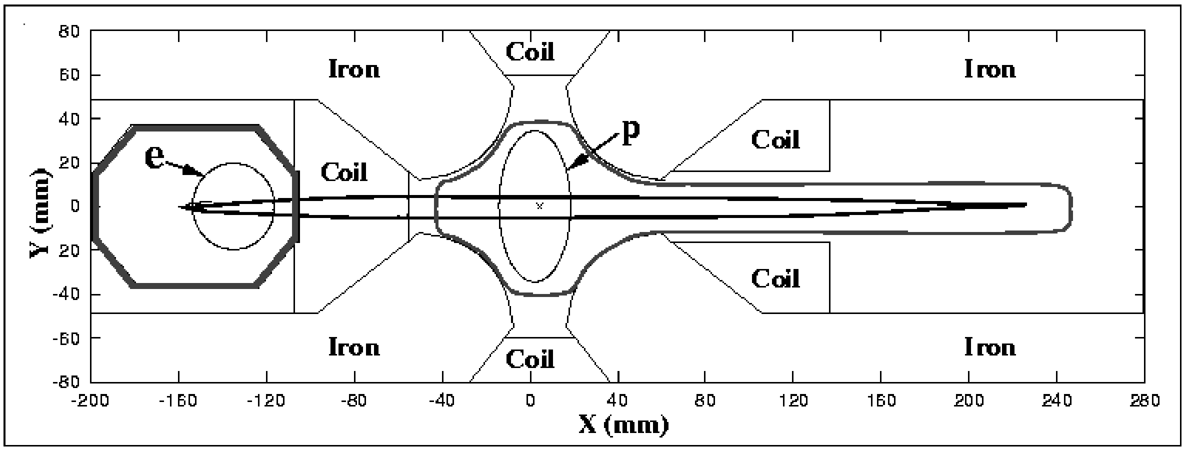

Figure 15: Aperture required at downstream end of first QN, Fig. 5 section **GG**.

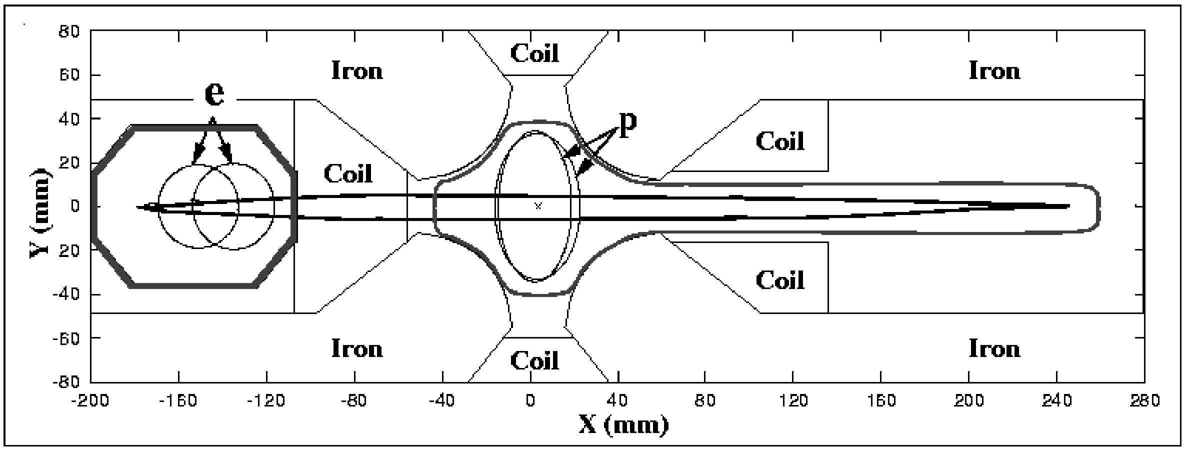

Figure 16: Aperture required at upstream and downstream ends of second QN, Fig. 5 sections **GG and HH**.

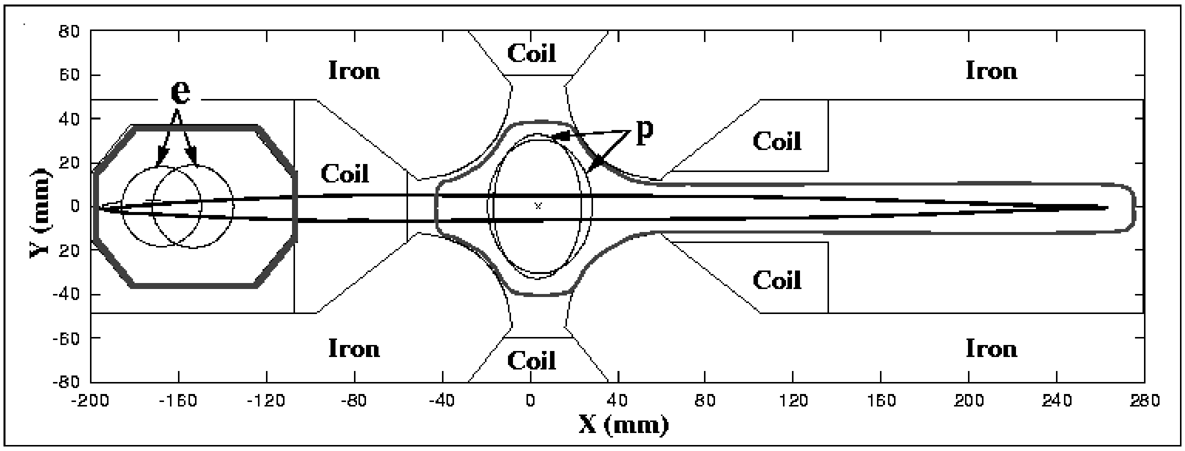

Figure 17: Aperture required at upstream and downstream ends of third QN, Fig. 5 sections **HH and II**.

6.2 Rev. 2–Lattice with Superconducting Combined Function Magnets Inside the Detectors

The separation of the electron (positron) beam from the proton beam is accomplished by magnetic separation. In order to separate the two beams as quickly as possible, the corresponding magnets have to be installed inside the colliding beam detector. They deflect the electron beam by $8\,mrad$. The choice of this angle is a compromise between strong separation field and tolerable background due to back-scattered photons from the downstream synchrotron radiation absorbers. In addition, to avoid detrimental chromatic effects in the focusing of the electron beam, the separator magnets also have a noticeable gradient field to provide early focusing. Integrated gradients of $4.2\,T$ are required to provide about one half of the necessary vertical focusing of the electron beam so that the separator magnet constitutes the first magnet of a low β triplet.

One of the largest problems of the separators is the limited space available, in particular in the transverse plane. At several locations, the detectors offers only an opening of $180\,mm$ diameter for these magnets. At the same time, the magnets cannot be placed too close to the interaction point (IP) in order to avoid shadowing detector elements mainly in the upstream direction ("upstream" refers to the direction of the electron beam, it is also referenced as "forward" direction, the direction of the average boost of particle produced in e–p collisions).

As a compromise between the need to provide separation and focusing as early as possible and preserving the acceptance of the detector, the upstream magnets will be placed at a distance of $1.9\,m$ from the IP. On the downstream side, at a distance of $1.6\,m$ from the IP is chosen. Using the remaining space inside the detector,about $3.5\,m$ length is available for the separators. The average field to produce a deflection of $8mrad$ for a $30GeV$ positron beam is then $0.23T$ and average gradients of $12T/m$ are needed.

While the outer dimensions of the separators must be kept within tight limits, the aperture of the these magnets must be rather large. On the upstream side, an aperture of $90\,mm$ is needed to provide space for the electron beam ($20\sigma_x$ correspond to a horizontal beam envelope at the upstream end of the upstream magnet of $31\,mm$ for $\beta_x^* = 0.64\,m$). On the downstream side, the aperture must not only contain the electron beam but also the synchrotron radiation fan produced inside the IR magnets. On the extreme downstream end, the aperture must be as large as $150mm$.

In order to meet all these constraints and requirements, a superconducting magnet design has been chosen. Despite the fact, that superconducting magnets add a lot of technical complication to this already complicated environment, they offer the only technically attractive solution to the problem.

6.2.1 Rev 2 Interaction Region Geometry

The geometry and dimensions of these magnet is described as follows. Since the field in a quadrupole varies with transverse distance from the centre and since the field may not vary too strongly to avoid excessive synchrotron radiation (a field strength of about $0.28\,T$ is found to be close to the limit tolerable), a natural choice is to align the quadrupoles along the direction of the beam orbit. Since the sagitta of the orbit is small ($3.5\,mm$), a straight magnet is considered which has a tilt of $4\,mrad$ with respect to the beam direction in the IP which is also the detector axis. However, it turns out that this arrangement is only possible in the upstream case. In the downstream case, where the magnet needs to provide aperture for the synchrotron radiation fan, it appears to be more favourable to align the separator along the detector axis. In order to allow for a reasonable installation procedure, the downstream magnets have to split in two halves. This is also desirable for the following reasons: Since the aperture needs to be increased with increasing distance from the IP, the constraints can be better met by building two downstream magnets with different apertures. This is in particular true since on the far downstream end, there is virtually no transverse space limitation since this is the location of the present superconducting compensator solenoid and the corresponding cryogenic supplies. Furthermore, it is desirable to control the dipole component of the field independently in the two magnets to avoid too strong magnetic fields on the beam orbit.

Thus, the set up consists of three magnets, two (e-beam) downstream magnets and one up-stream magnet. A considerable advantage of the arrangement is that it is the same for for H1 and ZEUS despite quite different boundary conditions. It allows a collision point in the center of the colliding beam detectors. This however is only possible if all the available margin of free space is used up in case of the H1 detector (see below). The upstream magnet, named "QO" has a length of 3.5 m. It starts at $1.9\,m$ upstream of the IP. The cryostat is centered on the detector axis at a distance of $3.8\,m$ from the IP which is in the middle of the two welds of the H1 liquid Argon cryostat. These welds limit the available space in the case of H1. The magnet is rotated around a point between these welds in the horizontal plane by an angle of $4\,mrad$. Then the downstream end of this magnet which occurs at $1.9\,m$ is shifted by 7.6mm outwards in the horizontal plane. The beam, which is centred on the detector axis at the IP has a horizontal displacement of $-7.6\,mm$ (inwards) with respect to the magnet axis at both ends. In order to provide the necessary deflection and focusing, the magnets has a quadrupole field of $G = 0.12\,T/m$ and, in addition, a dipole field of about $B = 0.18\,T$. It should, however, be noticed, that in the case of H1, the available space for this arrangement is extremely tight. The aperture limiting welds of the liquid Argon calorimeter cryostat are loacated at $4.6\,m$ upstream from the IP, and at $2.8\,m$ from the IP respectively. These welds leave a circular opening of only $190\,mm$ for installing the magnets. This limits the magnet outer dimension to a circle of $88\,mm$. For the $4\,mrad$ tilt a total space of $4\,mrad \times 1.8\,m = 7.2\,mm$ is needed in the horizontal plane. The rest of the available aperture is only $6.8\,mm$. It is available to make up for mechanical tolerances and for the sag of the cryostat under the influence of its own weight.

The aperture of the magnet for the beam is $90\,mm$ which is about $28\,mm$ more than needed for $20\sigma_x$ of the electron beam.

The first downstream quadrupole, named "QG" has a length of 2m. It is aligned parallel to the detector axis but shifted outwards by $27\,mm$ with respect to the detector axis. The corresponding $-27\,mm$ offset of the beam to the quadrupole axis provides the space necessary for the synchrotron radiation fan. The gradient of this magnet is $G = 13\,T/m$. An additional dipole field of $B_d = -0.13\,T$ on the axis of the quadrupole is needed. It weakens the field from the quadrupole and provides the right amount of deflection of $4.7\,mrad$. This limits the maximum field seen by the beam to $B_b = 0.27\,T$. In addition, it is assumed that a field of $0.1\,T$ is available to provide correction possibilities and to maintain flexibility for minor design changes. The extension of the beam orbit upstream of the detector which is a line with a horizontal slope of $8\,mrad$ with respect to the detector axis marks the border of the high power synchrotron radiation fan generated inside the separator magnets. It has a clearance of $25\,mm$ from the aperture (half aperture is 55mm). Within $18\,mm$ from the $8\,mrad$-line, the intensity

Element	QO	QG	QH
magnetic length	3.5 m	2.0 m	1.6 m
Maximum Gradient	12 T/m	13 T/m	11 T/m
Dipole Field in the Center	0.18 T	0.15 T	0.13 T
Outside Diameter	168 mm	178 mm	400 mm
Closest Distance to IP	1.9 m	1.6 m	3.9 m
Maximum Field seen by the Beam	0.27 T	0.27 T	0.27 T
Aperture	90 mm	110 mm	150 mm
Horizontal Tilt	4 mrad	0 mrad	0 mrad
Horizontal shift from Detector Axis	7.6 mm	27 mm	21 mm
k-value in Rev. 2	0.11 m^{-2}	0.12 m^{-2}	0.10 m^{-2}
bend radius in Rev. 2	577 m	-833 m	-1000 m

Table 5: Main Parameters of the Superconducting Separator Magnets

of the synchrotron radiation is expected to drop by three orders of magnitudes. The 20σ beam envelope has a clearance of about 10mm from the inside aperture limit.

The second downstream magnet, named "QH", follows the first one with a 30 cm drift space in between to provide space for coil heads and cryogenic supplies. It has a length of 1.6 m. It needs a very large aperture of 150 mm to provide room for the deflected beam and, on the opposite site, for the synchrotron radiation fan. The magnet is aligned along the detector axis and is shift outwards by $21mm$. The free space between the border of the synchrotron radiation fan and the outer aperture is about 24 mm. The beam stay-clear on the inside is about 10 mm. The gradient of this magnet reaches up to $G = 11\,T/m$. The dipole field on the beam orbit needs to be weakened by a dipole field of $B_d = -0.1\,T$. The total deflection of the electron beam by these two magnets is 8 $mrad$.

The set-up is shown in fig6.5.5.

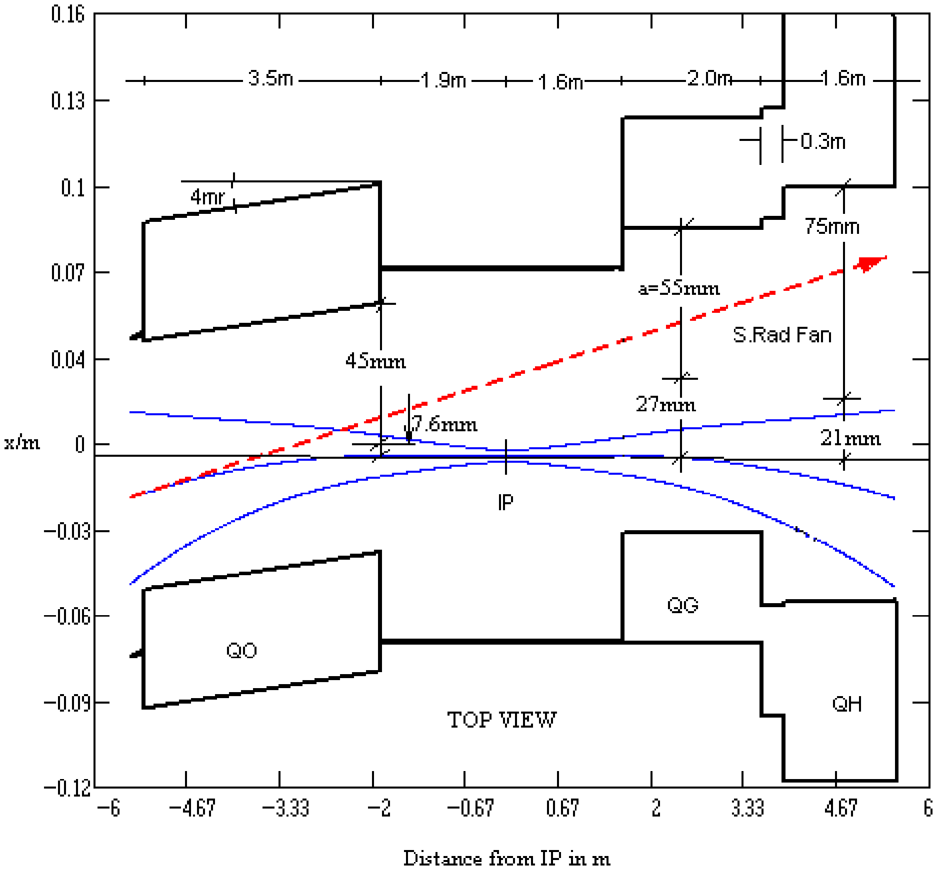

Figure 18: Schematic top view of the set up of superconducting focusing and deflection magnets in the colliding beam detector: The beams collide in the centre of the detector. The $20\sigma_x$ electron beam envelope is shown. The $3.5\,m$ long upstream quadrupole magnet is tilted by $4\,mrad$ in the horizontal plane. Its downstream end is shifted by $7.6\,mm$ from the detector (collision) axis. Its integrated gradient is $42\,T$. In addition it has a dipole field of $0.18\,T$. The total deflection of the e-beam inside is $8mrad$. On the downstream side, there are two quadrupole magnets aligned on the detector axis. They are shifted from the axis by $27\,mm$ and $21\,mm$ respectively and they need a dipole component to provide the correct amount of deflection of $8\,mrad$.